Ligand solid-solution tuning of magnetic and mechanical properties of van der Waals metal-organic magnet $NiCl_2(btd)_{1-x}(bod)_x$

Emily Myatt[1], Simrun Lata[1], Jem Pitcairn[1], Dominik Daisenberger[2], Silva M. Kronawitter[3], Sebastian A. Hallweger[3], Gregor Kieslich[3], Stephen P. Argent[1], Jeremiah P. Tidey[4], and Matthew J. Cliffe [*1]

[1]School of Chemistry, University of Nottingham, University Park, Nottingham, NG7 2RD, United Kingdom
[2]Diamond Light Source, Chilton, Didcot OX11 0DE, United Kingdom
[3]TUM Natural School of Sciences, Technical University of Munich, D-85748 Garching, Germany
[4]Department of Physics, University of Warwick, Gibbet Hill Road, Coventry, CV4 7AL, United Kingdom

October 21, 2024

Contents

[*]matthew.cliffe@nottingham.ac.uk

List of Figures

List of Tables

S1 Synthesis

All starting materials and solvents were purchased from standard chemical suppliers: 2,1,3-benzothiadiazole, btd (Acros 98%), 2,1,3-benzoxadiazole (ABCR, 97%), Nickel(II) chloride hexahydrate (Alfa Aesar 98%). ^{1}H NMR spectra were recorded in DMSO-d6 on a Bruker Ascend 400 or Bruker Avance (III) HD 400.

S1.1 Solid state synthesis $NiCl_2(btd)_{1-x}bod_x$

A typical synthesis is given below for $x_t = 0.5$. $NiCl_2 \cdot 6\,H_2O$ 965.0 mg (4.06 mmol) was ground with stoichiometric ratio of ligand: bod 254.6 mg (2.12 mmol) and btd 290.0 mg (2.13 mmol) until homogeneous. The reaction mixture was then added to a 23 mL PTFE liner and placed in a Parr autoclave, where it was heated at 200°C for 3 days to produce a lime green free-flowing microcrystalline powder.

S1.2 Solution synthesis $NiCl_2(btd)_{1-x}bod_x$

A typical synthesis is given below for $x_t = 0.5$. A solution of $NiCl_2 \cdot 6\,H_2O$ (105 mg, 0.442 mmol) in ethanol (0.8 mL) was heated to 70°C. A ligand solution containing bod 33.9 mg (0.282 mmol) and btd 39.5 mg (0.290 mmol) in ethanol (0.1 mL) was then added to the Ni(II) solution with stirring and heating over a period of 1 minute. Lime green microcrystalline powder precipitated immediately and the solvent was removed under vacuum. The samples were washed with ethanol (3 x 5 mL) to remove $NiCl_2 \cdot 6\,H_2O$ impurities where appropriate.

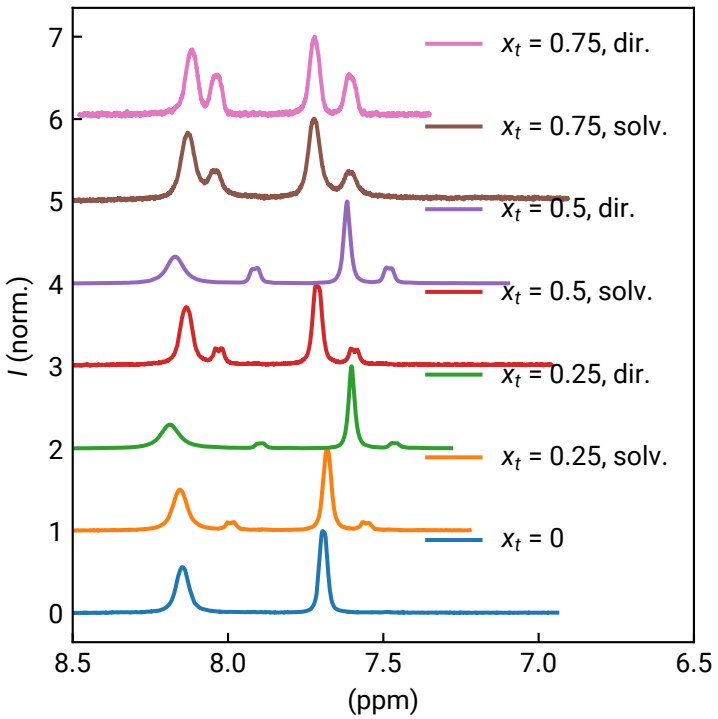

Figure S1: Solution ^{1}H NMR of digested solid-solution samples in d_6-DMSO. x_t = target composition, solid = synthesised using direct solid state reaction; soln. = solution synthesis.

S2 Diffraction characterisation

S2.1 Ambient Pressure Laboratory PXRD

Powder X-ray diffraction measurements were performed on a Malvern PANalytical Xpert Pro diffractometer using monochromatic Cu Kα1 ($\lambda = 1.540562$ Å) radiation, operating at a tube voltage of 40 kV and tube current of 40 mA in Bragg Brentano geometry. The powder samples were loaded and flattened onto silicon plates. Pawley refinement was carried out using Topas Academic v6.[4] The sample peak shape was refined using a Thompson-Cox-Hastings pseudo-Voigt peak shape, and the lattice parameters were refined without additional constraints. The background was represented by a six term Chebyshev polynomial and a very broad peak (FWHM $> 5^{\circ}$) and a sample height correction was applied.

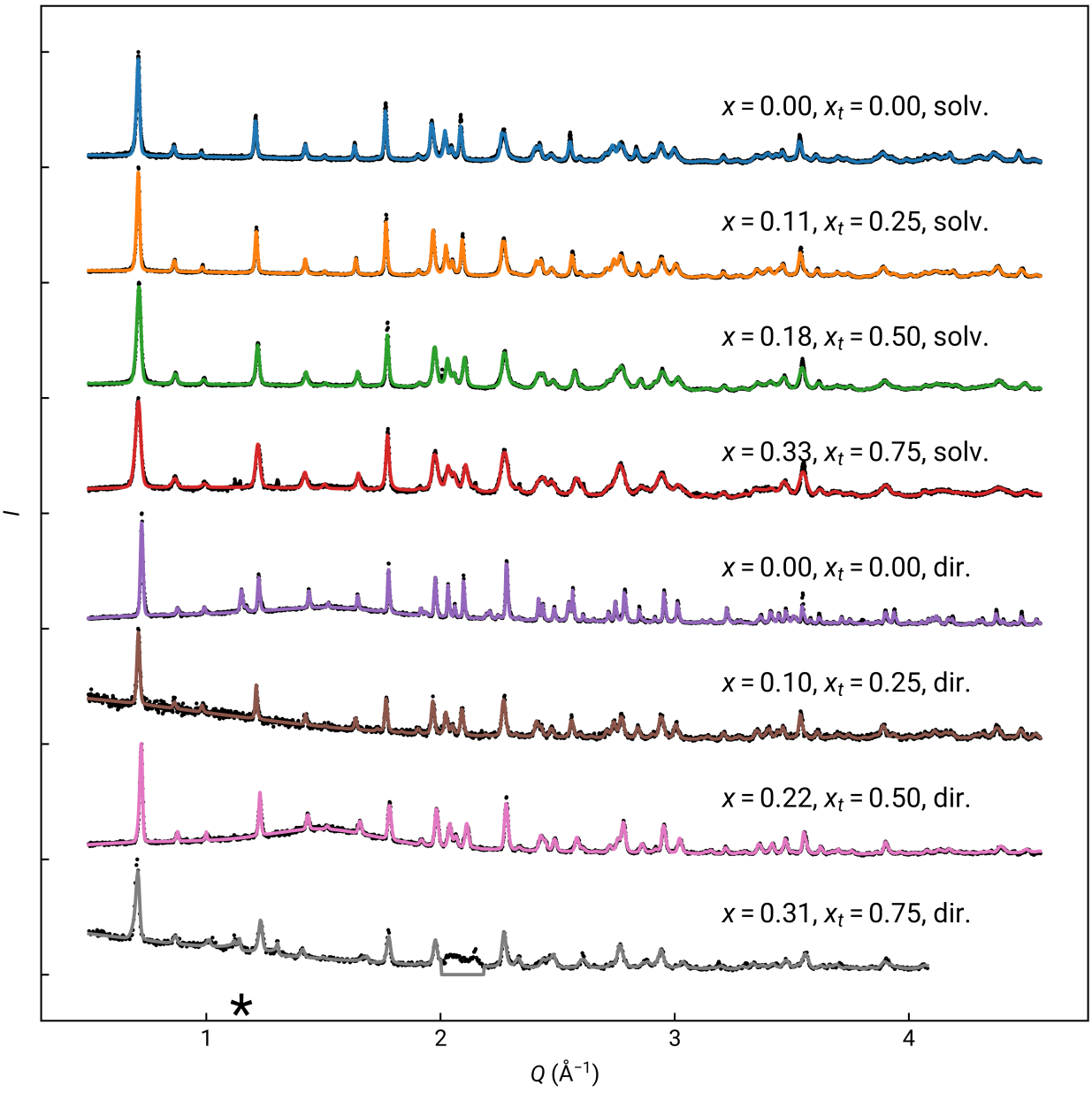

Figure S2: Stack plot of laboratory PXRD data set for all samples with Pawley refinement shown.

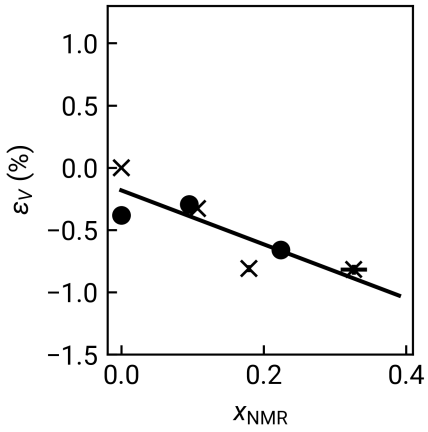

Figure S3: Plot showing the evolution of volumetric strain determined by Pawley refinement for all samples.

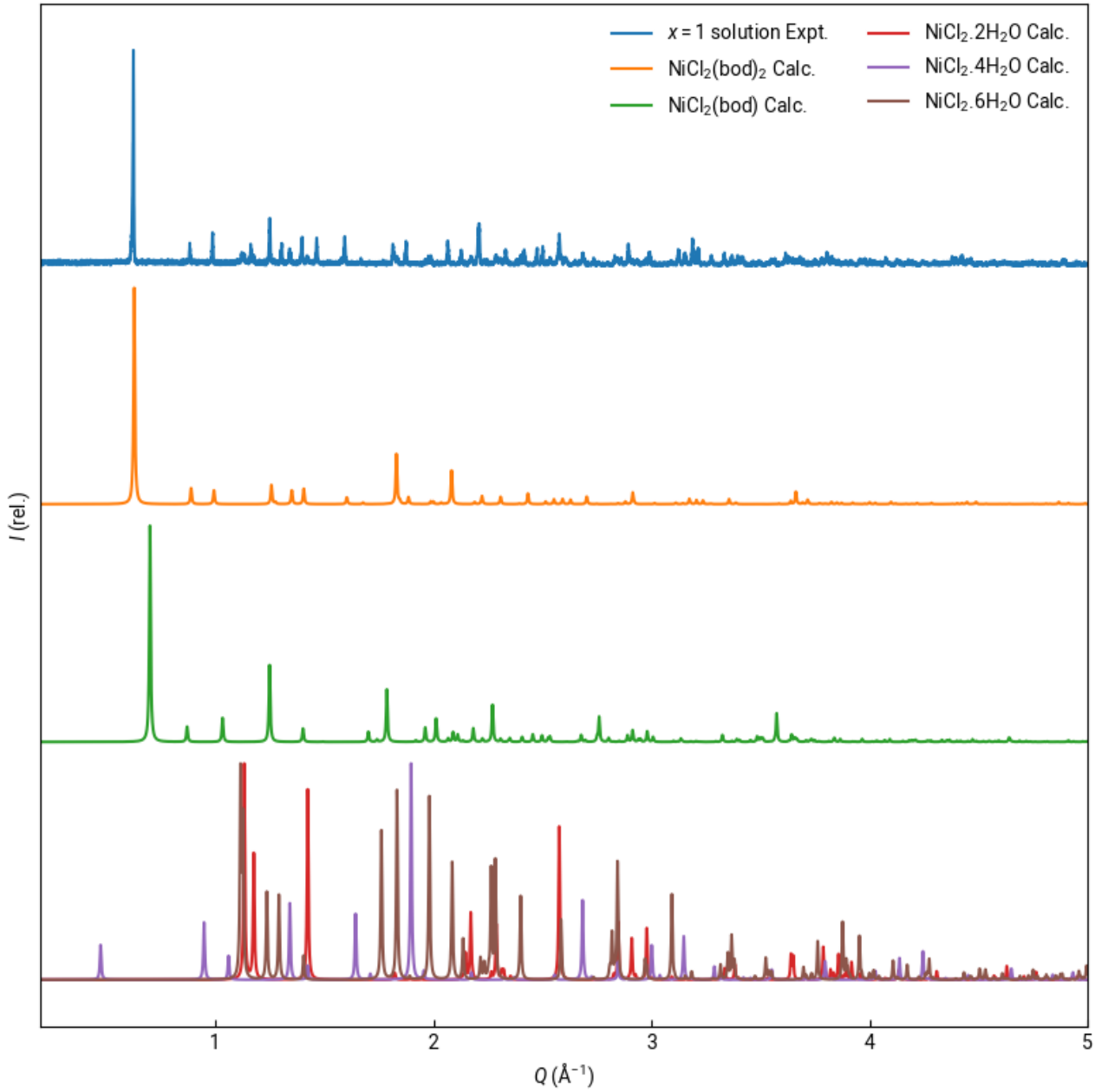

Figure S4: Comparison of laboratory PXRD dataset for $x_t = 1$ synthesised in solution. The Python Matador package was used for PXRD calculation.[1]

S2.2 High pressure synchrotron PXRD

High pressure synchrotron powder X-ray diffraction (HP-PXRD) was performed at beamline I15 of Diamond Light Source (Oxford, UK, experiment number CY30815-2) using a monochromatic X-ray beam (λ = 0.4246 Å) and a Dectris Pilatus3 X CdTe 2M detector. Fine powders were packed into Makrolon capillaries (1.95 mm diameter) and evenly mixed with silicone oil AP-100 as a non-penetrating pressure transmitting medium (PTM) to ensure hydrostatic pressure. The capillaries were sealed with epoxy resin, loaded into a sample holder and inserted into a hydraulic high pressure cell. The pressure head of this system is a steel block in which the sample holder sits, access to X-rays is provided by two opposing diamond windows located on the upstream (X-ray source) and downstream (X-ray detector) sides of the steel block. A motorised software-controlled syringe pump is used to pressurise the water in the steel-block sample-enclosure, pressures are determined directly via strain-gauge sensors. Pump operation and pressure readings are linked via the control software and hence desired pressures can be directly set. The overall pressure range for HP-PXRD was from ambient to 0.4 GPa, with pressure steps of 0.02 GPa. DAWN software was used to obtain diffraction patterns from images recorded by the detector in real time.[5]

Pawley refinement was carried out using Topas Academic v6 sequentially refining from the highest to lowest pressure.[4] The background was represented by a six term Chebyshev polynomial plus three very broad peaks (FWHM $\approx 1^{\circ}$) to account for the structured background from pressure transmitting medium and sample cell. The sample peak shape was refined using a Thompson-Cox-Hastings pseudo-Voigt peak shape, and the lattice parameters were refined without additional constraints. For $x = 0$, small impurity peaks were accounted for using two independently refining peaks.

Table S1: Fitted compressibilities and bulk moduli using PASCal[3] for $NiCl_2(bod)_x(btd)_{1-x}$ samples directly synthesised through solid state synthesis.

x	$K(X_1)$ (TPa^{-1})	$K(X_2)$ (TPa^{-1})	$K(X_3)$ (TPa^{-1})	B (GPa)
0	27.3(3)	14.8(4)	7.7(4)	18.7(3)
0.1	24.7(4)	12.6(2)	8.14(16)	20.6(3)
0.2	24.70(11)	14.1(3)	8.9(4)	19.96(13)

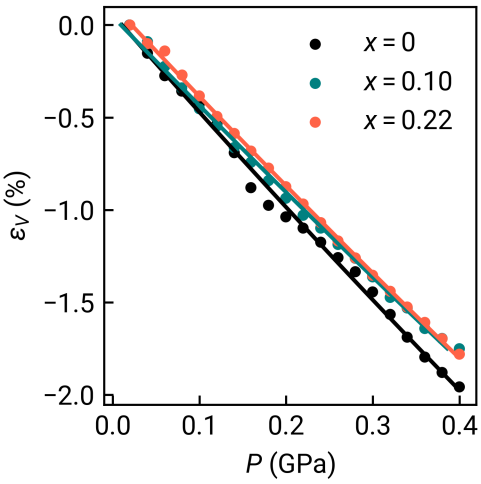

Figure S5: Volume as a function of pressure determined by high pressure synchrotron PXRD, fitted by the second order Birch-Murnaghan equation of state.[2]

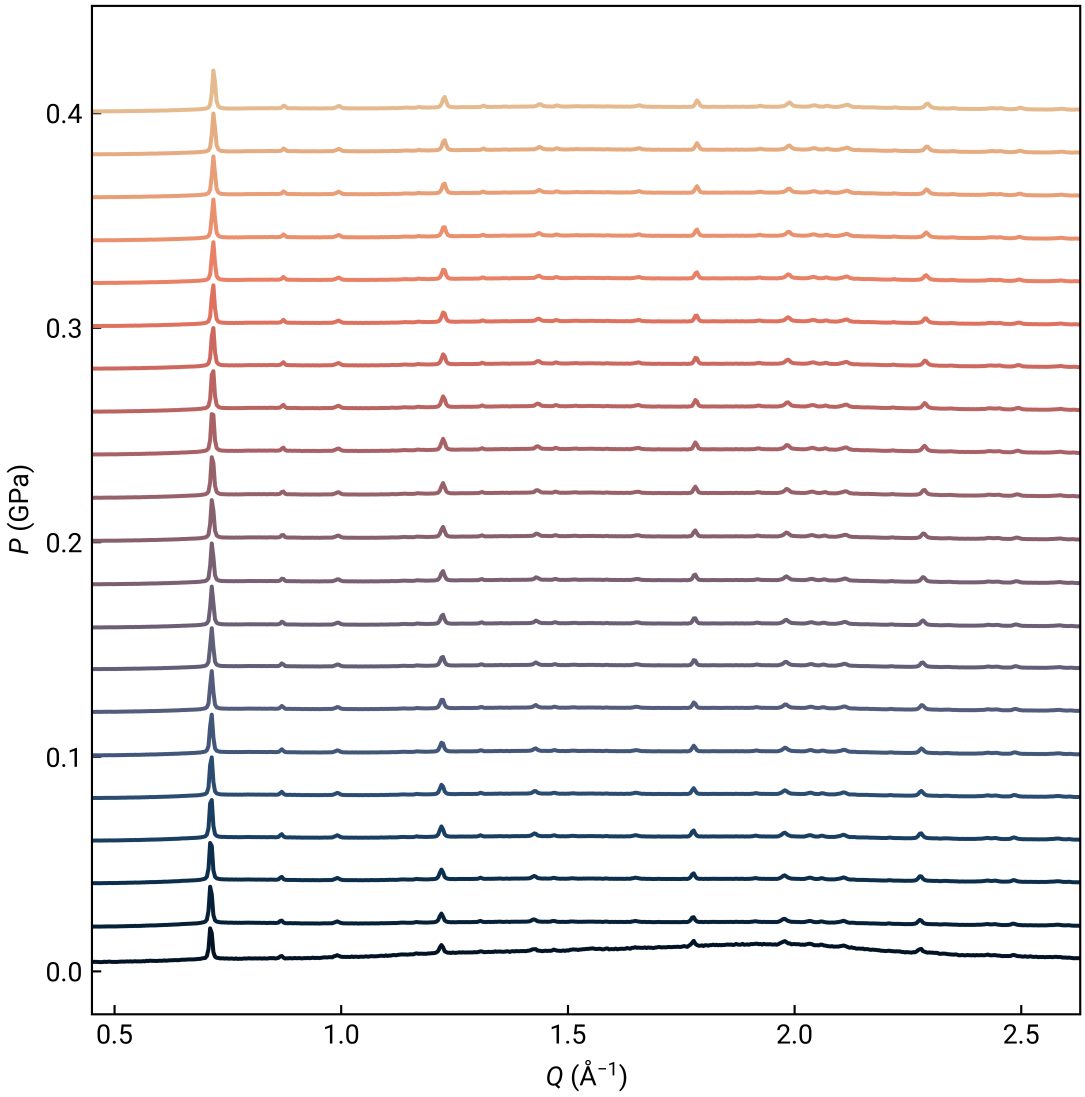

Figure S6: Stack plot of high pressure synchrotron PXRD data set for $x = 0$ synthesised directly in the solid state.

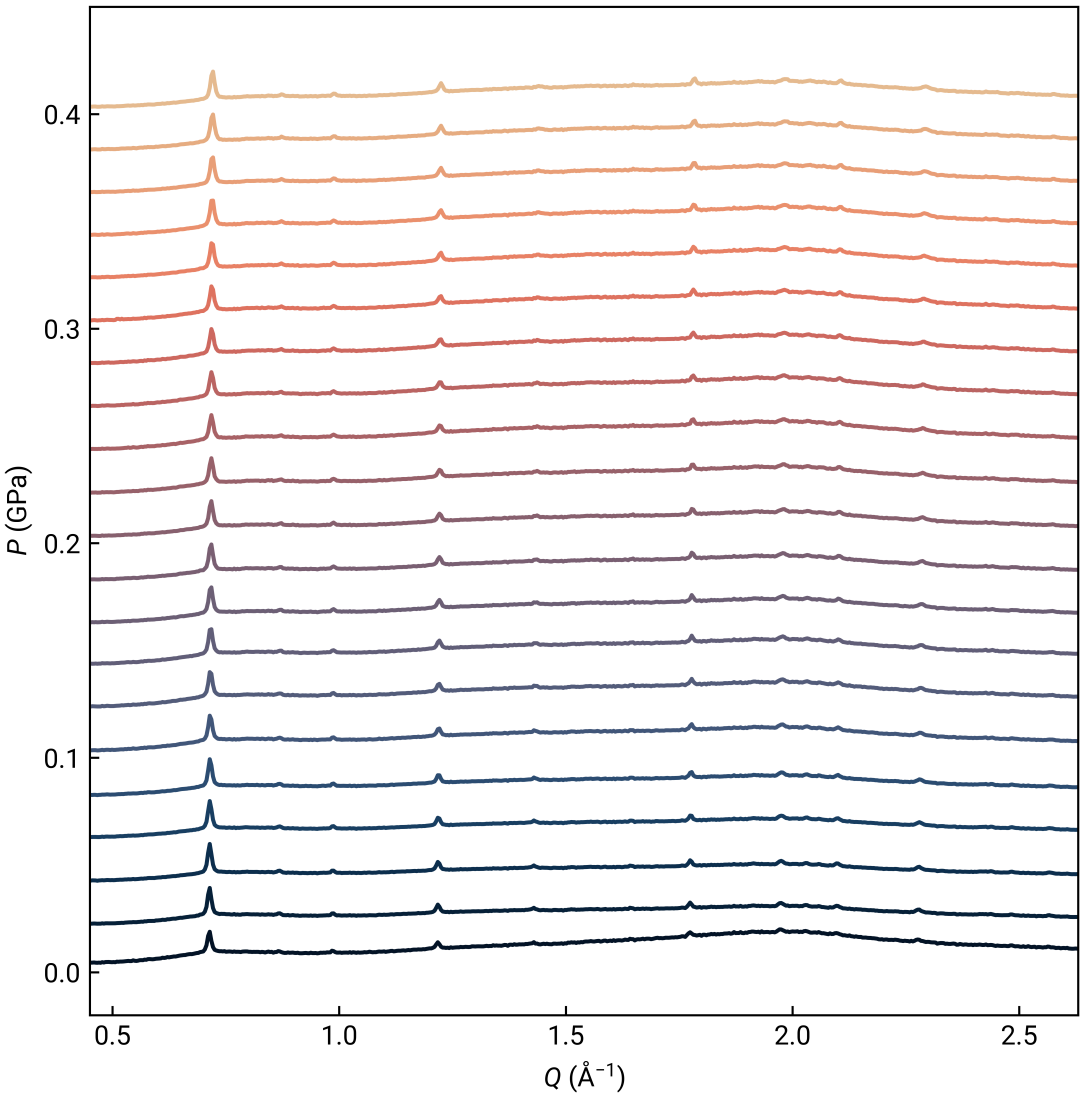

Figure S7: Stack plot of high pressure synchrotron PXRD data set for $x = 0.1$ synthesised directly in the solid state.

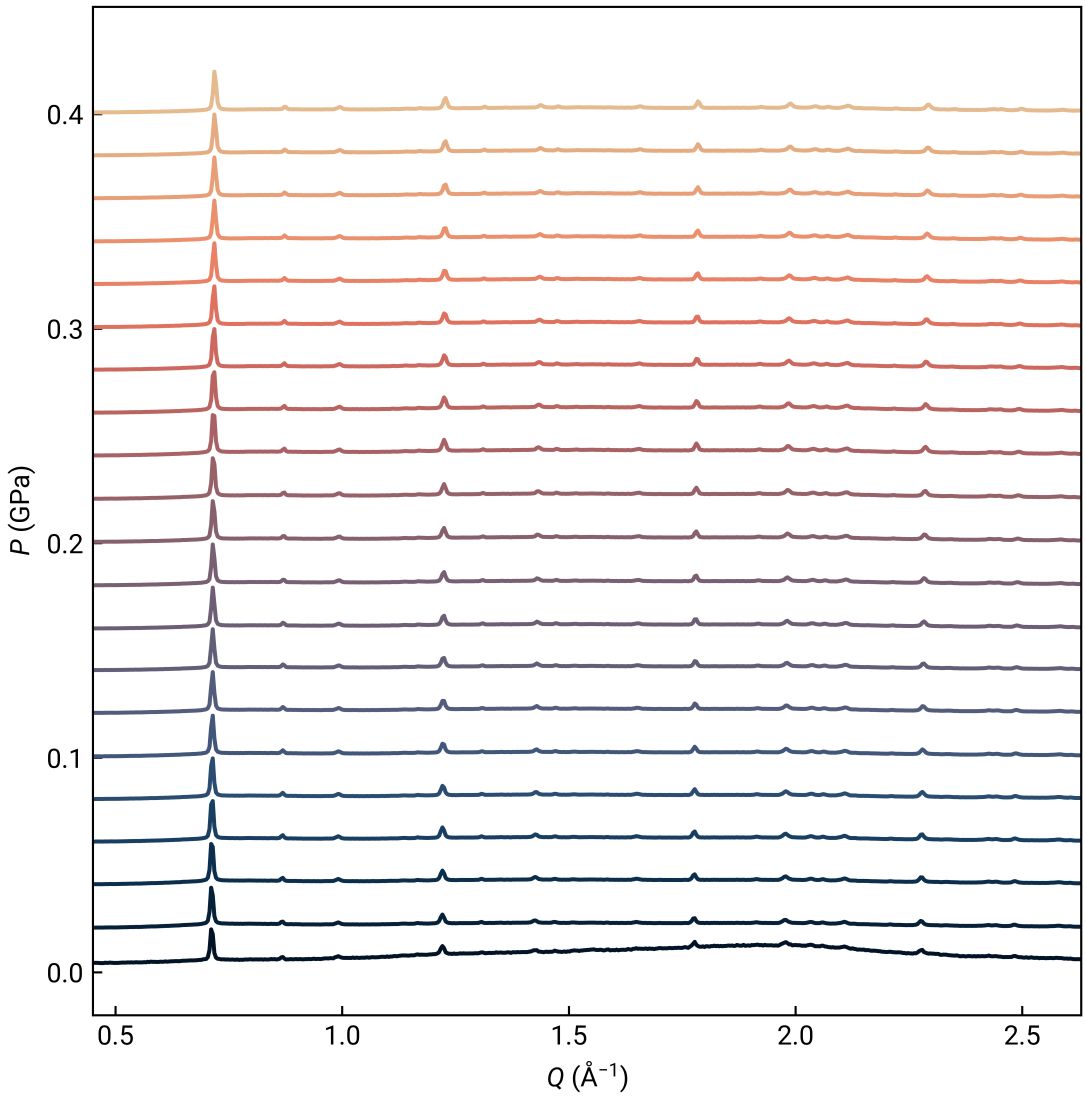

Figure S8: Stack plot of high pressure synchrotron PXRD data set for $x = 0.2$ synthesised directly in the solid state.

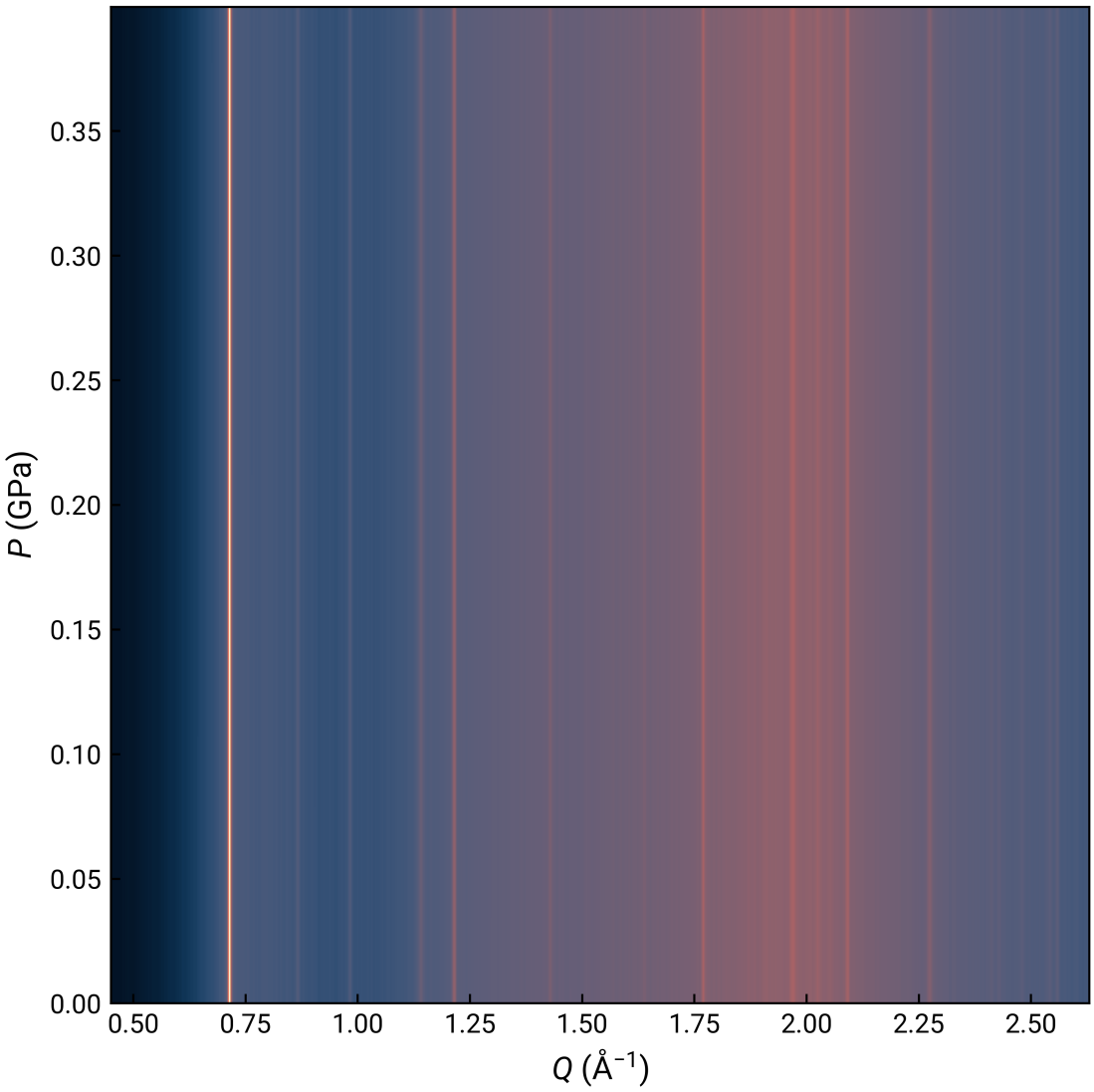

Figure S9: Heat map plot of high pressure synchrotron PXRD data set for $x = 0$ synthesised directly in the solid state.

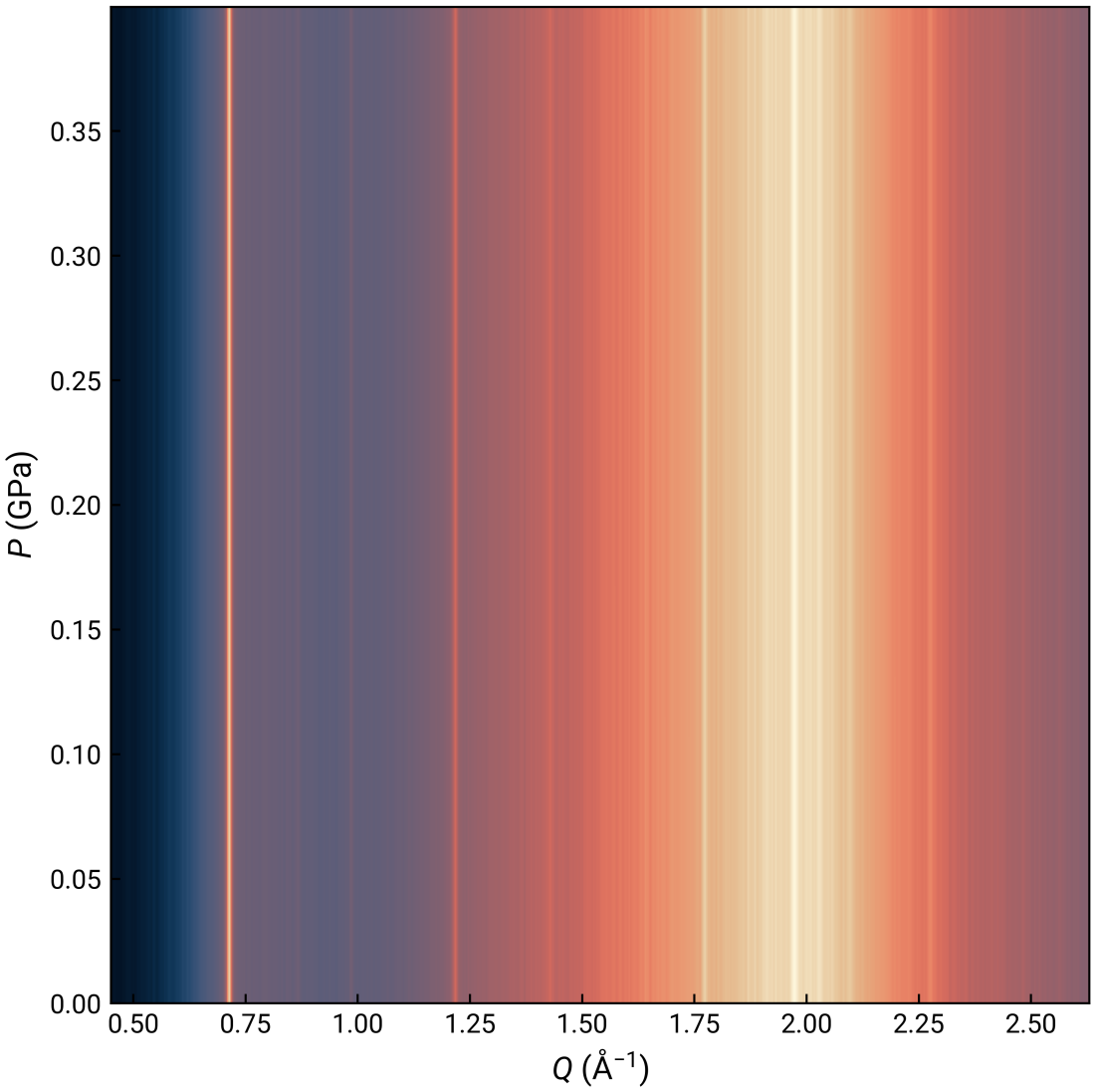

Figure S10: Heat map plot of high pressure synchrotron PXRD data set for $x = 0.1$ synthesised directly in the solid state.

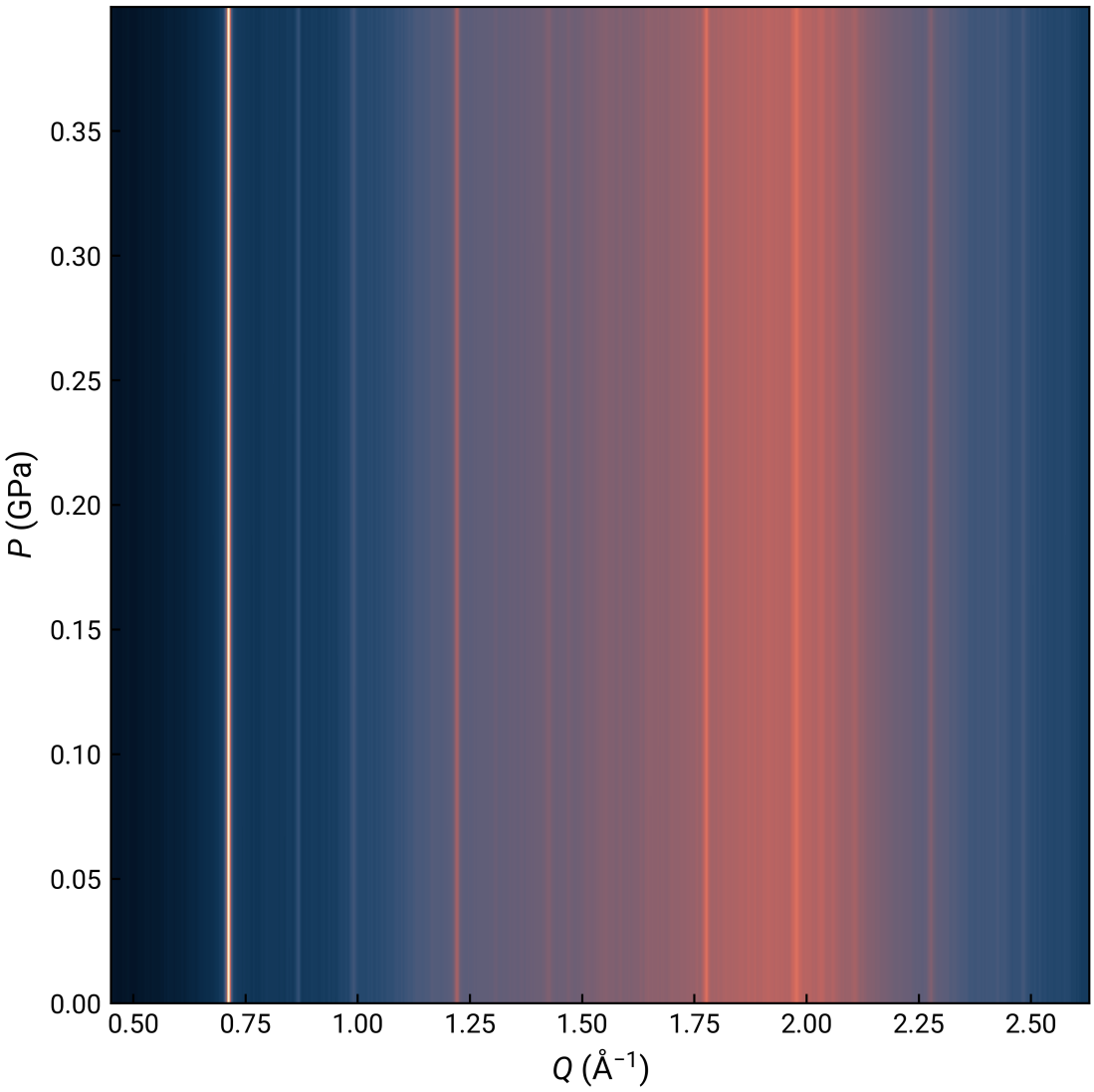

Figure S11: Heat map plot of high pressure synchrotron PXRD data set for $x = 0.2$ synthesised directly in the solid state.

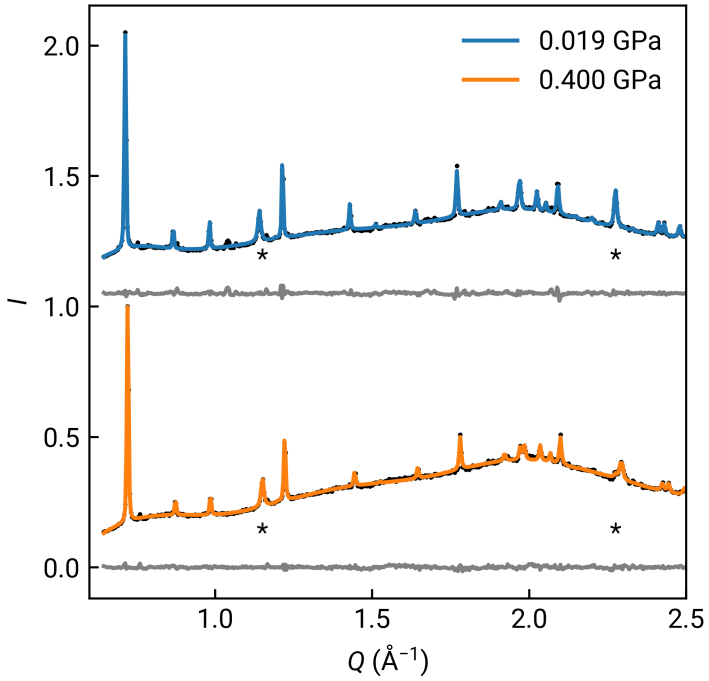

Figure S12: Pawley refinement of high pressure synchrotron PXRD data sets at the lowest (0.02 GPa) and highest (0.4 GPa) pressures for $x = 0$ directly solid state synthesised. Data: black; fit: colour; difference: grey; impurity peaks marked by *.

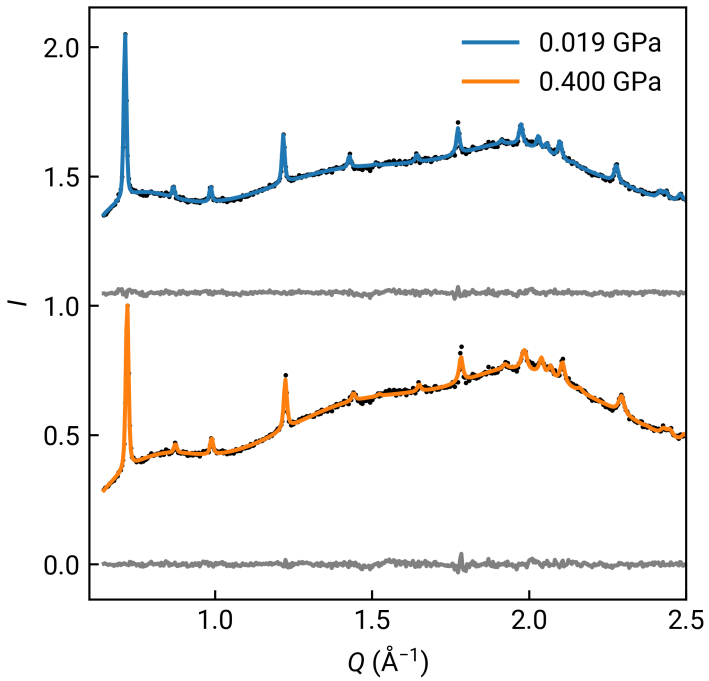

Figure S13: Pawley refinement of high pressure synchrotron PXRD data sets at the lowest (0.02 GPa) and highest (0.4 GPa) pressures for $x = 0.1$ directly solid state synthesised. Data: black; fit: colour; difference: grey.

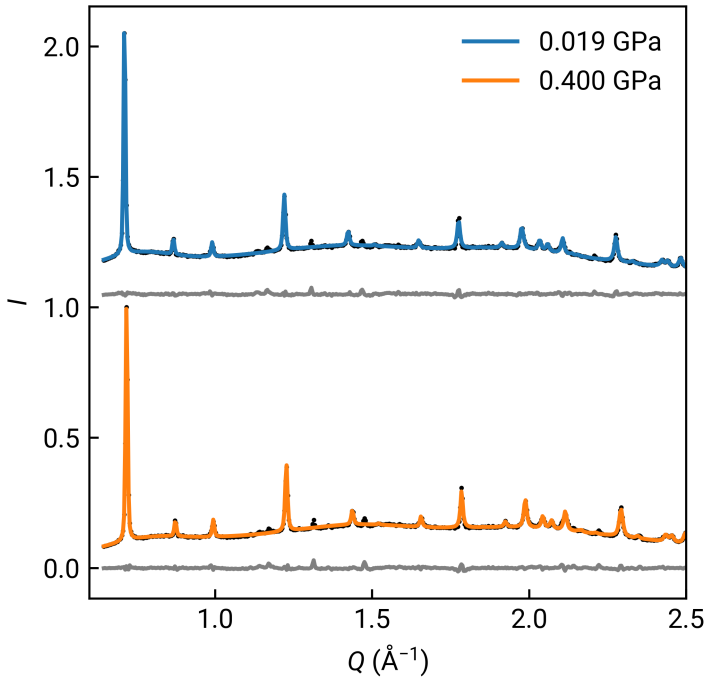

Figure S14: Pawley refinement of high pressure synchrotron PXRD data sets at the lowest (0.02 GPa) and highest (0.4 GPa) pressures for $x = 0.2$ directly solid state synthesised. Data: black; fit: colour; difference: grey.

Table S2: Lattice parameters derived by Pawley refinement for $x = 0.0$, direct solid state.

P (GPa)	R_{wp}	a (Å)	b (Å)	c (Å)	β (°)	V (Å^3)
0.000	1.378	3.5486(6)	12.7827(12)	8.7928(5)	89.90(3)	398.85(8)
0.0193	2.032	3.5481(3)	12.7849(8)	8.7908(4)	89.887(11)	398.76(4)
0.0398	1.883	3.54618(18)	12.7815(6)	8.7845(4)	89.870(10)	398.16(3)
0.0598	1.871	3.54527(12)	12.7789(6)	8.7778(4)	89.868(10)	397.67(3)
0.0794	1.717	3.54455(17)	12.7775(6)	8.7732(3)	89.877(10)	397.34(3)
0.0994	1.55	3.5438(2)	12.7782(7)	8.7681(3)	89.880(10)	397.05(4)
0.1199	1.419	3.5425(3)	12.7759(8)	8.7637(3)	89.859(11)	396.63(4)
0.1399	1.437	3.5409(3)	12.7717(9)	8.7569(3)	89.857(15)	396.01(5)
0.1594	1.551	3.5388(3)	12.7648(9)	8.7501(3)	89.859(14)	395.26(5)
0.1794	1.711	3.5379(2)	12.7629(8)	8.7452(4)	89.858(11)	394.88(4)
0.1996	1.799	3.53737(19)	12.7626(7)	8.7412(4)	89.856(10)	394.63(3)
0.2196	1.768	3.53679(18)	12.7624(6)	8.7374(3)	89.863(9)	394.39(3)
0.2397	1.807	3.5360(2)	12.7615(6)	8.7331(3)	89.872(10)	394.08(4)
0.2597	1.779	3.5349(2)	12.7615(7)	8.7286(3)	89.865(12)	393.75(4)
0.2798	1.654	3.5340(3)	12.7609(7)	8.7245(3)	89.861(14)	393.45(4)
0.2997	1.534	3.5327(3)	12.7582(8)	8.7197(3)	89.857(15)	393.01(4)
0.3198	1.526	3.5315(2)	12.7544(8)	8.7147(3)	89.857(15)	392.53(4)
0.3397	1.52	3.5304(2)	12.7504(8)	8.7093(3)	89.849(15)	392.03(4)
0.3598	1.514	3.5292(3)	12.7480(9)	8.7042(3)	89.842(14)	391.60(4)
0.3798	1.493	3.5282(3)	12.7466(9)	8.7003(3)	89.837(16)	391.28(5)
0.3998	1.521	3.5275(4)	12.7452(9)	8.6961(3)	89.812(18)	390.96(5)

Table S3: Lattice parameters derived by Pawley refinement for $x = 0.1$, direct solid state.

P (GPa)	R_{wp}	a (Å)	b (Å)	c (Å)	β (°)	V (Å^3)
0.000	1.154	3.5422(14)	12.743(3)	8.8037(10)	89.9(4)	397.36(19)
0.0193	1.237	3.5414(7)	12.7366(20)	8.7997(6)	89.96(19)	396.92(10)
0.0398	1.275	3.5406(6)	12.7353(18)	8.7948(6)	89.96(18)	396.56(9)
0.0598	1.207	3.5390(7)	12.7318(19)	8.7894(6)	89.9(3)	396.03(10)
0.0793	1.221	3.5380(7)	12.7285(19)	8.7840(7)	89.9(2)	395.57(10)
0.0996	1.187	3.5366(9)	12.726(2)	8.7790(7)	89.9(2)	395.12(13)
0.1199	1.173	3.5356(9)	12.725(3)	8.7742(8)	89.9(2)	394.75(13)
0.1399	1.167	3.5344(8)	12.721(2)	8.7692(7)	89.93(19)	394.29(12)
0.1594	1.19	3.5338(8)	12.719(2)	8.7652(7)	89.93(15)	393.97(12)
0.1794	1.196	3.5326(8)	12.717(2)	8.7610(7)	89.92(14)	393.58(12)
0.1996	1.171	3.5316(8)	12.715(2)	8.7568(7)	89.91(14)	393.20(12)
0.2196	1.138	3.5308(10)	12.712(3)	8.7525(8)	89.91(18)	392.84(14)
0.2397	1.155	3.5303(10)	12.710(3)	8.7485(8)	89.90(16)	392.56(15)
0.2597	1.154	3.5293(10)	12.709(3)	8.7441(9)	89.88(19)	392.21(15)
0.2798	1.142	3.5286(10)	12.708(3)	8.7403(8)	89.90(17)	391.91(15)
0.2997	1.153	3.5275(10)	12.705(3)	8.7357(8)	89.9(3)	391.51(14)
0.3198	1.143	3.5260(10)	12.703(3)	8.7313(8)	89.86(11)	391.08(14)
0.3397	1.165	3.5257(9)	12.702(2)	8.7277(8)	89.85(10)	390.85(13)
0.3598	1.158	3.5241(9)	12.699(2)	8.7237(7)	89.87(13)	390.41(12)
0.3798	1.179	3.5238(8)	12.698(2)	8.7202(7)	89.85(8)	390.19(11)
0.3998	1.192	3.5233(9)	12.696(2)	8.7179(7)	89.9(2)	389.97(13)

Table S4: Lattice parameters derived by Pawley refinement for $x = 0.2$, direct solid state.

P (GPa)	R_{wp}	a (Å)	b (Å)	c (Å)	β (°)	V (Å^3)
0.000	1.323	3.5363(8)	12.6718(19)	8.8204(4)	90.03(13)	395.26(11)
0.0194	1.846	3.5377(3)	12.6724(10)	8.8220(3)	90.02(6)	395.50(5)
0.0398	1.934	3.5368(3)	12.6695(9)	8.8174(3)	90.02(12)	395.11(4)
0.0598	2.112	3.5366(3)	12.6726(9)	8.8122(3)	90.02(13)	394.95(4)
0.0797	2.024	3.5352(3)	12.6676(9)	8.8076(3)	90.02(19)	394.43(4)
0.0996	1.996	3.5341(3)	12.6640(9)	8.8030(3)	90.02(9)	393.98(4)
0.1199	2.027	3.5327(3)	12.6616(9)	8.7983(3)	90.02(7)	393.55(4)
0.1399	2.049	3.5319(3)	12.6588(8)	8.7942(3)	90.03(12)	393.18(4)
0.1593	2.089	3.5309(3)	12.6572(9)	8.7892(3)	90.03(6)	392.80(4)
0.1794	2.03	3.5300(3)	12.6553(9)	8.7848(3)	90.03(5)	392.44(4)
0.1996	2.02	3.5289(3)	12.6525(9)	8.7805(3)	90.04(6)	392.05(4)
0.2196	2.016	3.5279(3)	12.6506(9)	8.7760(3)	90.04(7)	391.67(4)
0.2397	2.04	3.5270(3)	12.6475(9)	8.7715(3)	90.04(9)	391.28(4)
0.2597	2.048	3.5258(3)	12.6451(9)	8.7673(3)	90.04(8)	390.89(4)
0.2798	2.069	3.5249(3)	12.6429(9)	8.7630(3)	90.04(8)	390.52(4)
0.2997	2.073	3.5238(3)	12.6405(9)	8.7589(3)	90.04(7)	390.15(4)
0.3198	2.082	3.5229(3)	12.6386(9)	8.7549(3)	90.04(7)	389.80(4)
0.3397	2.111	3.5220(3)	12.6372(9)	8.7506(3)	90.05(6)	389.47(4)
0.3598	2.103	3.5211(3)	12.6350(9)	8.7470(3)	90.05(5)	389.14(4)
0.3798	2.151	3.5200(3)	12.6328(9)	8.7431(3)	90.05(5)	388.79(4)
0.3998	2.198	3.5190(3)	12.6314(9)	8.7394(3)	90.05(5)	388.46(5)

S2.3 Single crystal X-ray diffraction

A suitable crystal of $NiCl_2(bod)_2$ was selected from the product of solution reaction with $x_t = 1.0$, mounted in air and analysed on an Agilent Diffraction SuperNova(II) diffractometer, equipped with an Titan S2 CCD area detector diffractometer. The crystal was kept at 120(2) K during data collection using an Oxford Cryosystems open flow liquid nitrogen Cryostream cooler. Using Olex2,[6] the structure was solved with the ShelXT structure solution program using a dual-space algorithm[7] and refined with the ShelXL refinement package.[8]

The structure has been solved and refined in space group $P4_2bc$ with an asymmetric unit containing one complete benzoxadiazole ligand, one chloride ligand and half a nickel(II) cation. The PLATON tool ADDSYM suggests the presence of a new (pseudo) centre of symmetry and an alternative centrosymmetric space group $P4_2/mbc$. An attempt was made to solve and refine the structure in $P4_2/mbc$ with an asymmetric unit containing half a benzoxadiazole ligand disordered over a symmetry element, half a chloride ligand and quarter of a nickel(II) cation. The centrosymmetric solution featuring disordered overlapping benzoxadiazole ligand reflected a structure with the same connectivity as the non-centrosymmetric one, however, with a larger R_1 value ($P4_2/bc, R_1 = 5.07\%$ vs $P4_2/mbc, R_1 = 10.40\%$).

The Hooft parameter of 0.6(9) calculated for the weak data with a low resolution limit does not allow any conclusions to be drawn about the absolute configuration, if any, of the structure. The alternative disordered solution in centrosymmetric space group $P4_2/mbc$ indicates that the presence of inversion twinning is possible. Refining this $P4_2/bc$ structure as an inversion twin with a fixed or refined twin fraction did not result in a lower R_1 value so was not pursued.

The very small crystal diffracted weakly with a data resolution limit of 1.20 Å, resulting in a low data to parameter ration of 3.63. The structure could only be refined with anisotropic displacement parameters by way of applying rigid bond and similarity restraints on the atoms of the benzoxadiazole ligand (RIGU, SIMU). The anisotropic displacement parameter of carbon C7 was restrained to have more isotropic character (ISOR). The geometry of the benzoxadiazole ligand was restrained to be planer (FLAT). Irregular bond lengths around the phenyl ring of the ligand are likely a consequence of the weak data and ambiguity about missing symmetry discussed above. Attempts to restrain the benzoxadiazole ligand geometry to more reasonable and symmetrical values resulted in poor refinement convergence and distorted anisotropic displacement ellipsoids. It was decided to leave the geometry unrestrained and note that no detailed conclusions can be drawn from the ligand geometry other than the binding mode, connectivity and gross conformation of the structure.

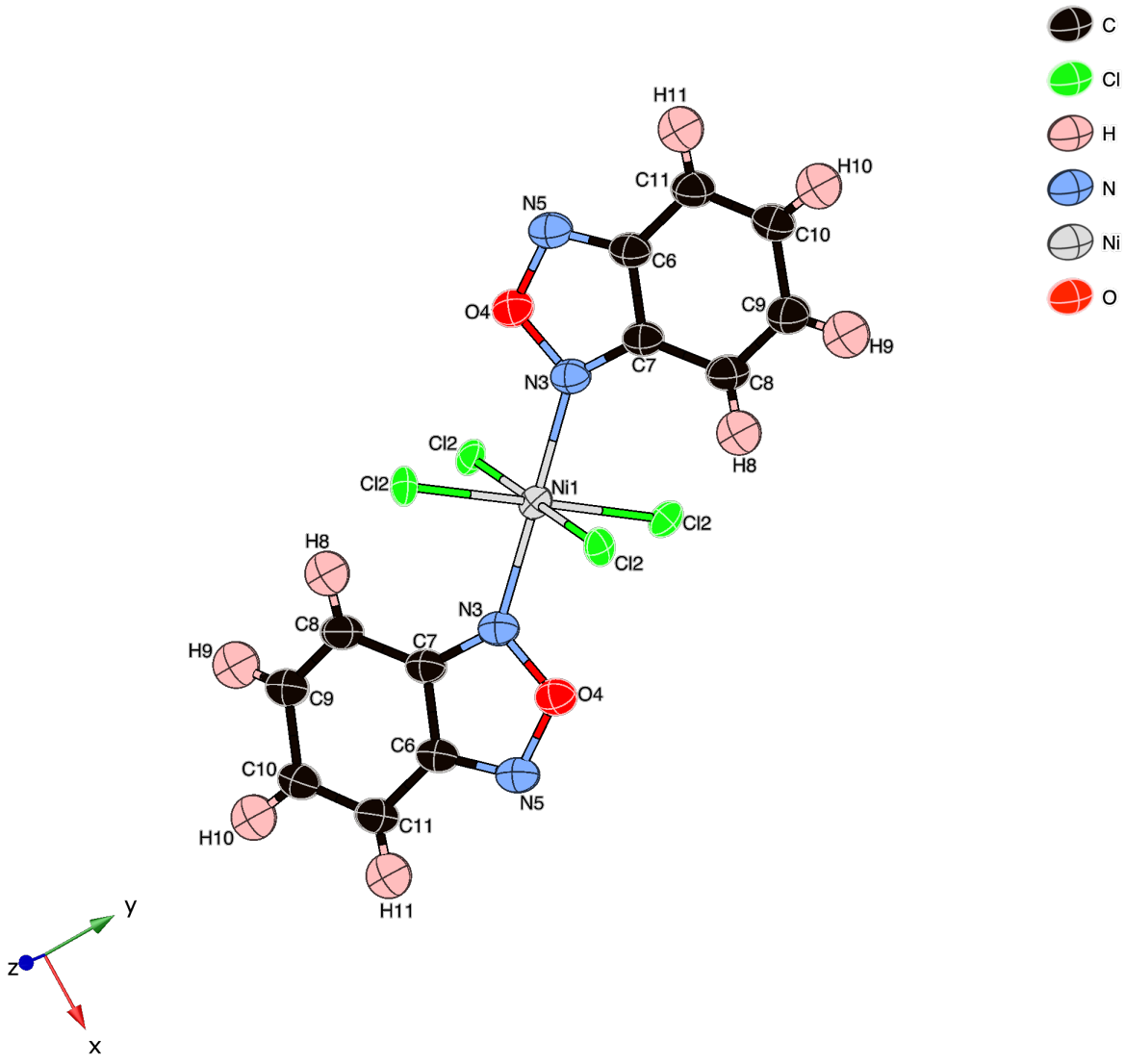

Figure S15: ORTEP of the X-ray single crystal structure of $NiCl_2(bod)_2$.

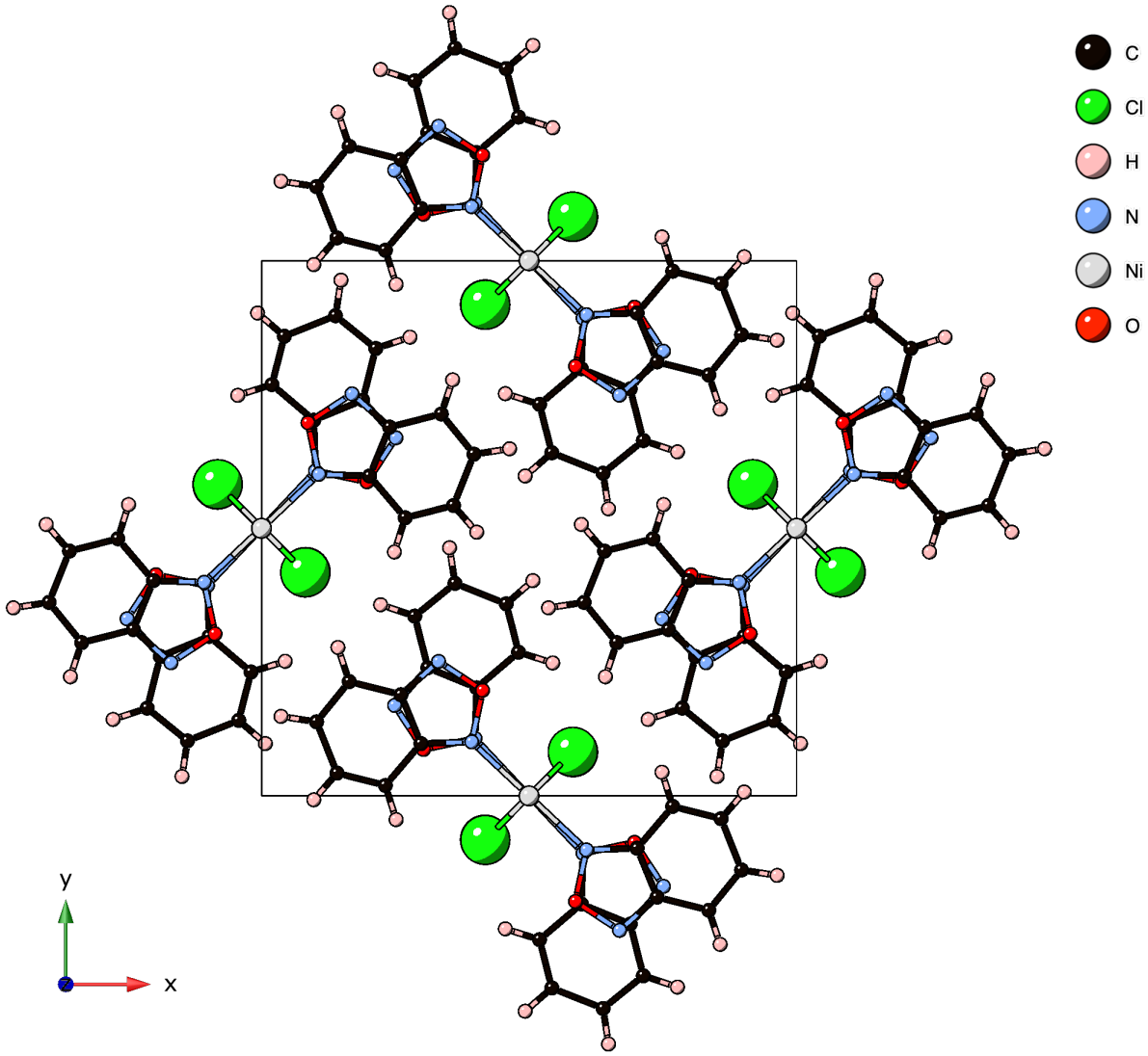

Figure S16: X-ray single crystal structure of $NiCl_2(bod)_2$ viewed along *c* showing the packing.

Table S5: Crystallographic details for X-ray diffraction structures for $NiCl_2(bod)_2$.

	$NiCl_2(bod)_2$
Chemical formula	$C_{12}H_8Cl_2N_4NiO_2$
M_r	369.83
Crystal system, space group	Tetragonal, $P4_2bc$
Temperature (K)	120
a, c (Å)	14.1275 (19), 6.8620 (14)
V (Å^3)	1369.6 (5)
Z	4
Radiation type	Cu $K\alpha$
μ (mm^{-1})	5.73
Crystal size (mm)	0.06 × 0.01 × 0.01
Diffractometer	SuperNova, Titan S2
T_{min}, T_{max}	0.837, 0.968
No. of measured, independent and observed [$I > 2\sigma(I)$] reflections	2409, 352, 214
R_{int}	0.111
θ_{max} (°)	39.9
(sin θ_{max}/λ) (Å^{-1})	0.416
$R[F^2 > 2\sigma(F^2)]$, $wR(F^2)$, S	0.051, 0.122, 1.06
No. of reflections	352
No. of parameters	97
No. of restraints	211
H-atom treatment	H-atom parameters constrained
$\Delta\rho_{max}$, $\Delta\rho_{min}$ (e Å^{-1})	0.33, -0.37
Absolute structure	Classical Flack method preferred over Parsons because s.u. lower.
Absolute structure parameter	0.0 (3)

S2.4 Single crystal electron diffraction

For the single crystal electron diffraction experiments, a portion of the solution reaction product with $x_t = 1.0$ was lightly ground between glass slides, dispersed onto a copper-supported holey carbon grid and loaded via a Gatan Elsa cryo holder into a Rigaku XtaLAB Synergy-ED electron diffractometer, operated at 200 kV and equipped with a Rigaku HyPix-ED hybrid pixel array area detector. Data for a range of crystallites were surveyed at ambient temperature (~293 K) using selected area continuous rotation electron diffraction with a selected area aperture of 2 µm diameter at the sample. A pair of closely related phases were found and data are reported in orthorhombic space group, $Pmma$ ($a = 12.67(7)$ Å, $b = 3.55(11)$ Å, $c = 8.81(9)$ Å), and as a non-merohedral, two-fold rotation twin of monoclinic space group, $P2/c$ ($a = 12.67(7)$ Å, $b = 3.55(11)$ Å, $c = 8.81(9)$ Å, $\beta = 93.05(15)°$), with data wedges of 135° and 140°, respectively, using 0.25° frames. Data were collected using CrysAlisPRO version 1.171.43.106a (Rigaku Oxford Diffraction, 2024), and indexed, integrated, and scaled using CrysAlisPRO version 1.171.43.121a (Rigaku Oxford Diffraction, 2024).

The structures were solved using ShelXT.[7] The orthorhombic structure was refined using Olex2 N-beam approach to handling multiple diffraction, while the monoclinic twin was refined in the kinematic approximation and using an extinction correction to handle an average impact of multiple diffraction with thirteen reflections omitted as extreme outliers; both structures are refined using Olex2.refine as implemented in Olex2,[6,9] version 1.5-ac6-020 (compiled 2024.02.14 svn.r2f8d729c for Rigaku Oxford Diffraction, GUI svn.r6920) using published scattering factors.[10]

It was determined through comparison of refinements employing pure btd, bod, and disordered systems, their statistical fit factors and bond lengths, that the monoclinic phase evidently comprised $NiCl_2$(bod) (i.e. $x = 1$). The orthorhombic phase was determined by the same approach to be a pure btd system $NiCl_2$(btd) (i.e. $x = 0$), although we cannot exclude the possibility of a small (<5%) inclusion of bod therein, suggestive of adventitious btd due to its high vapour pressure.

Global rigid bond restraints were employed, with a more tight restraint applied to the Ni-Cl bond of the orthorhombic phase to improve model stability. Hydrogen atoms were geometrically constrained at neutron bond distances, being refined with riding isotropic displacement parameters for the monoclinic phase, and fully anisotropic displacement parameters for the orthorhombic phase in the presence of similarity restrains to their parent atom.

These two new phases can be compared to the previously reported $NiCl_2$(btd) and $CoCl_2$(btd) structures which crystallise in $P2_1/m$.[11,12] The new orthorhombic polymorph of $NiCl_2$btd is the aristotype ($Pmma$), and is closely-related to the high temperature structure of $FeCl_2$(pym).[12] The previously reported $NiCl_2$(btd) structure breaks the a-glide $\perp c$ and $m \perp b$, retaining just the $m \perp a$ (which runs through the btd ligand), whereas the new $NiCl_2$(bod) phase in $P2/c$ only retains the $a \perp c$ (the cell setting having changed to the conventional), which lies in the $NiCl_2$(bod) layer. This suggests that the precise symmetry of these layered compounds will depend on synthesis conditions, and perhaps even particle size.

Complete experimental and refinement information are contained in the deposited CIFs along with structure factors and embedded .RES files, which are deposited in the CSD with CCDC reference codes, 2373766 and 2373767.

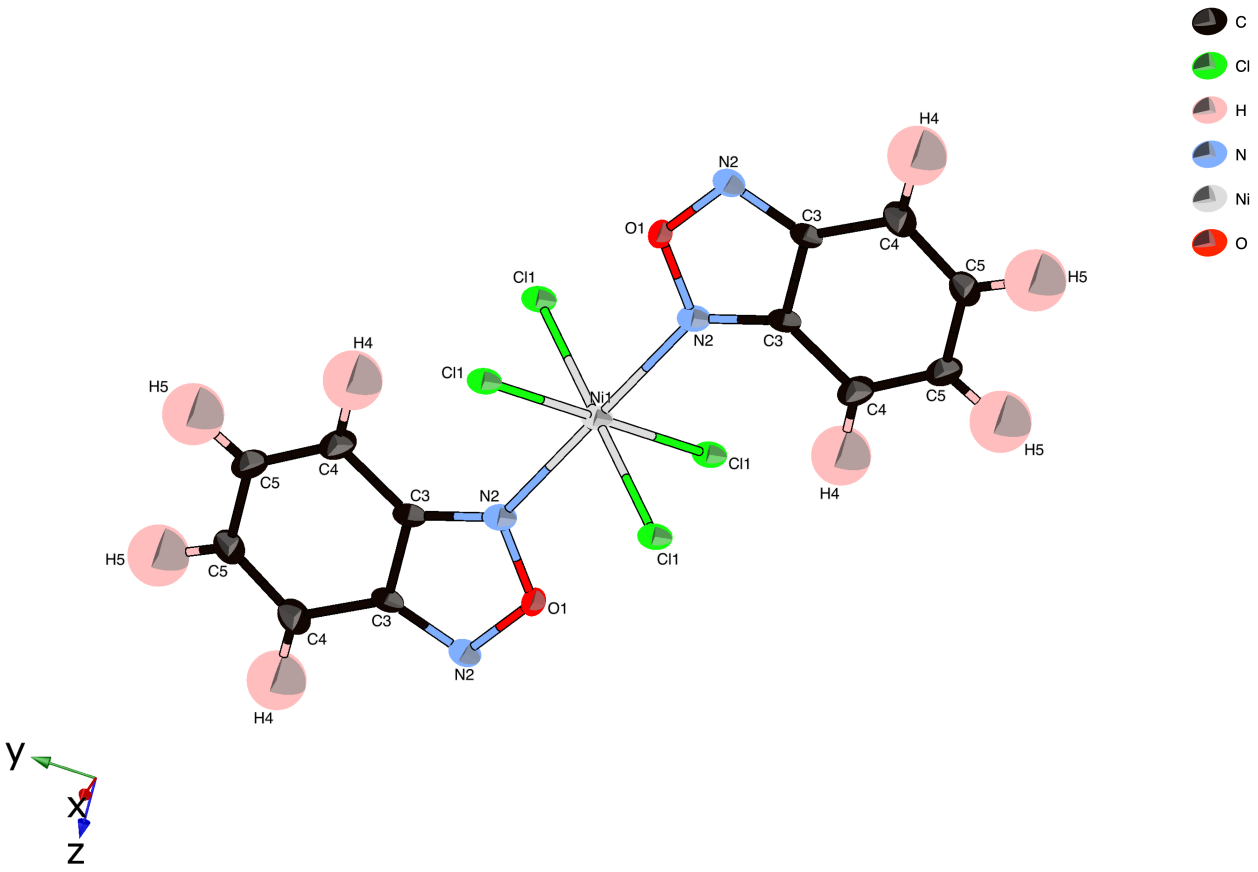

Figure S17: ORTEP of the electron single crystal structure of $NiCl_2$(bod).

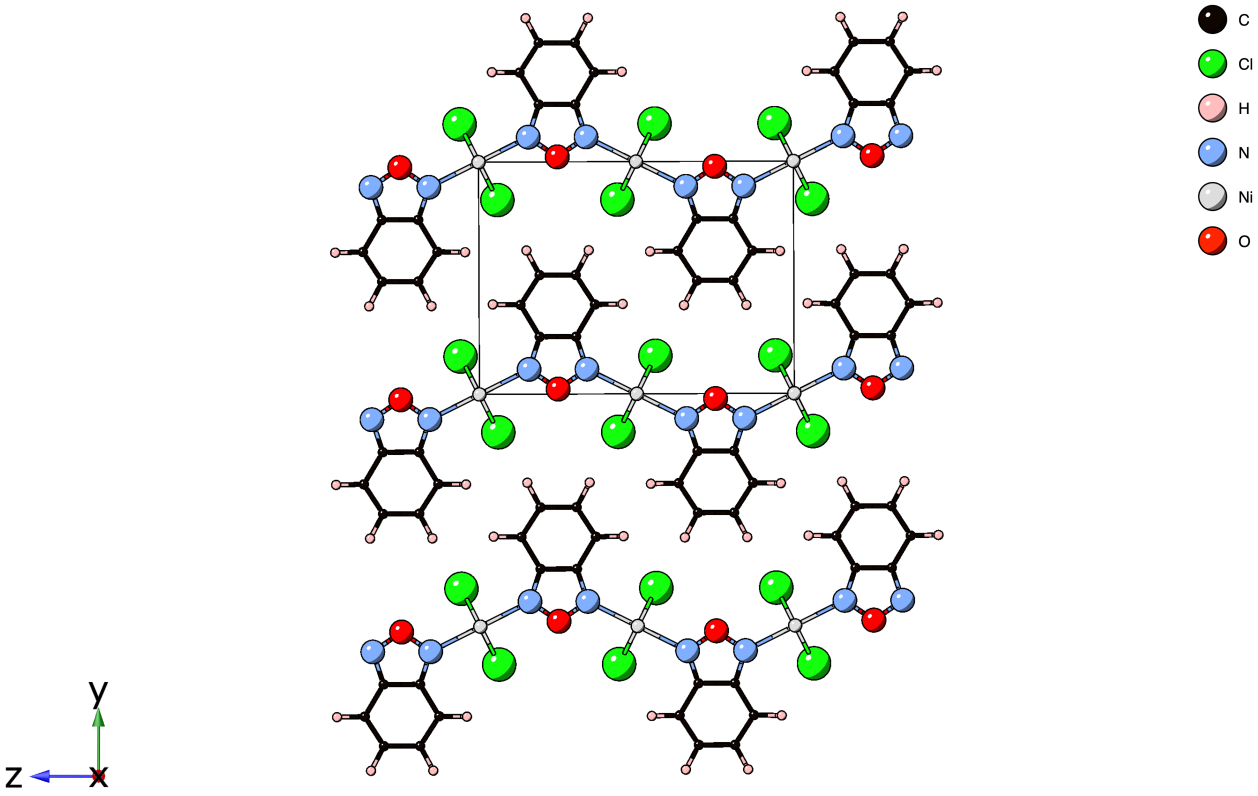

Figure S18: Electron single crystal structure of $NiCl_2$(bod) viewed along *a* showing the packing.

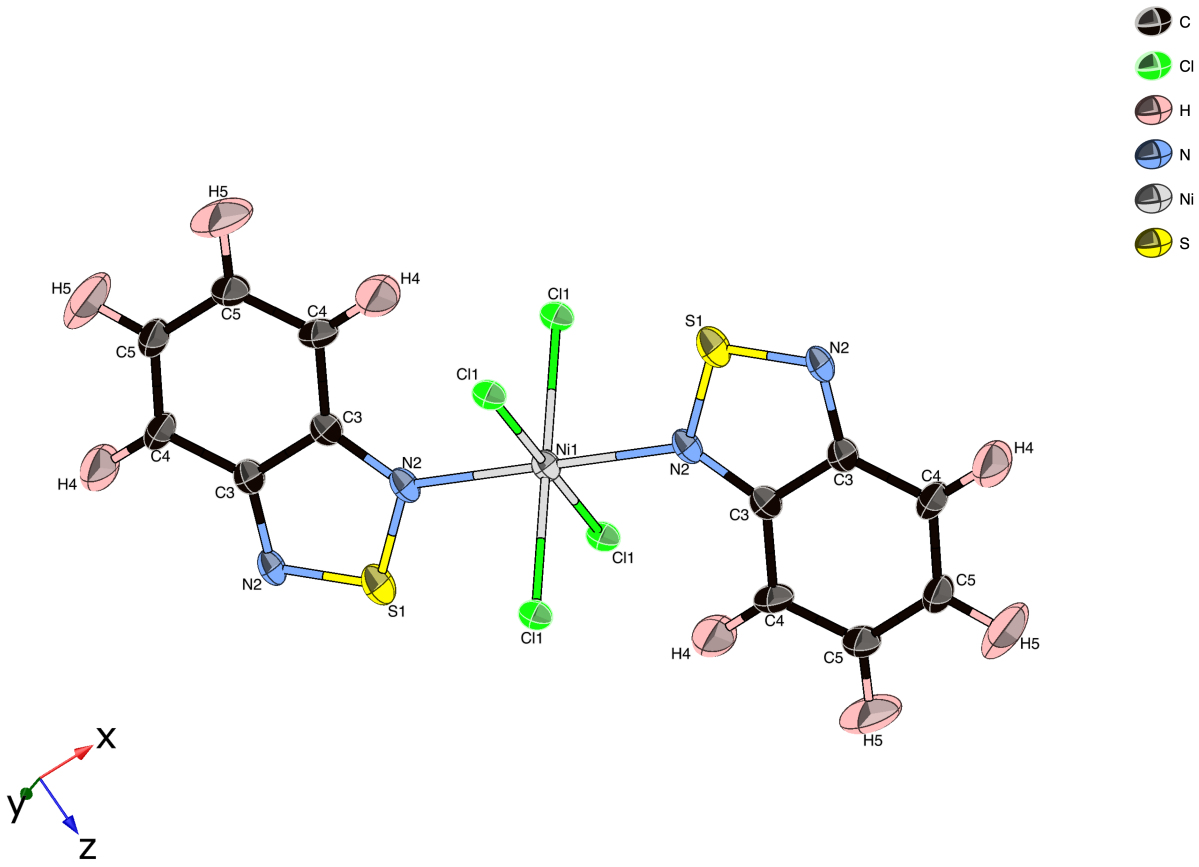

Figure S19: ORTEP of the electron single crystal structure of $NiCl_2$(btd).

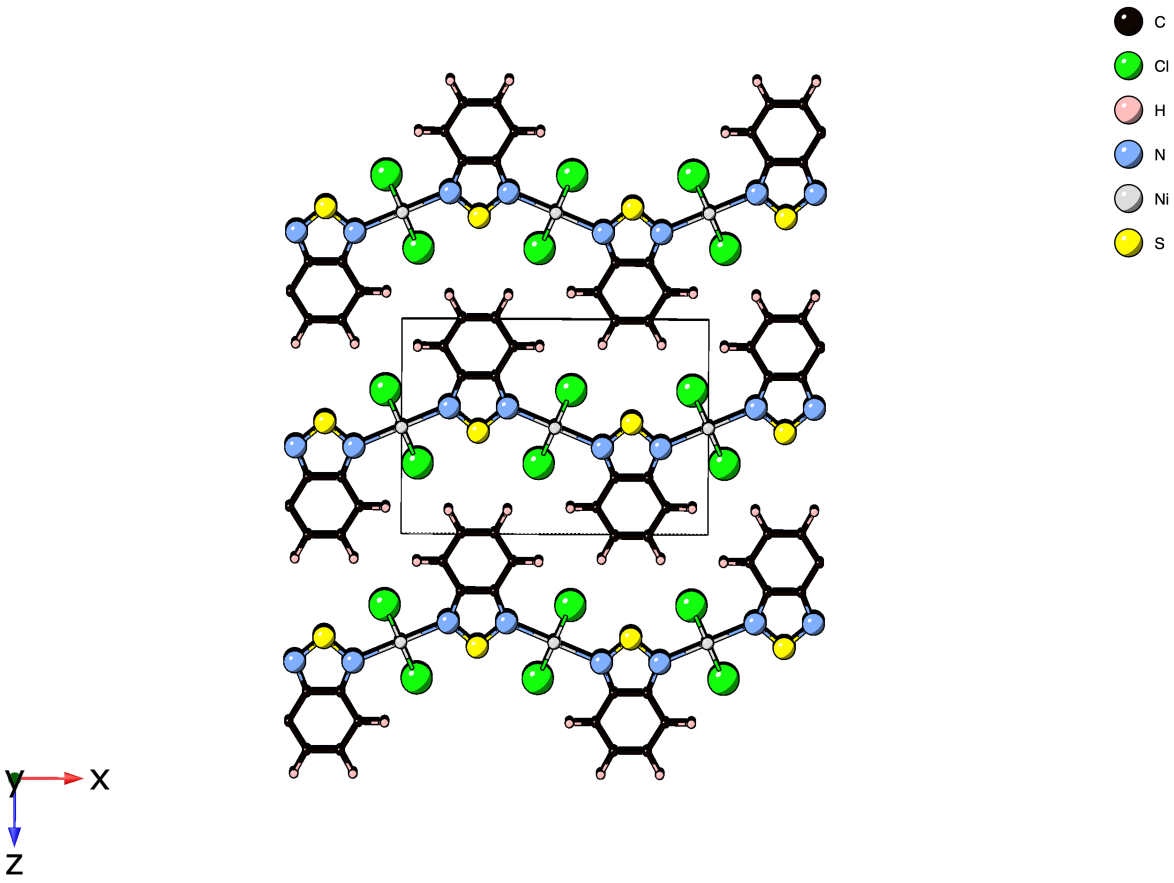

Figure S20: Electron single crystal structure of $NiCl_2$(btd) viewed along *b* showing the packing.

Table S6: Crystallographic details for electron diffraction structures for $NiCl_2$(bod) and $NiCl_2$(btd).

	$NiCl_2$(btd)	$NiCl_2$(bod)
Crystal data		
Chemical formula	$C_6H_4Cl_2N_2NiS$	$C_6H_4Cl_2N_2NiO$
M_r	265.78	249.71
Crystal system, space group	Orthorhombic, $Pmma$	Monoclinic, $P2/c$
T (K)	293(5)	293(5)
a, b, c (Å)	12.67(7), 3.55(11), 8.8 (9)	3.52(7), 8.96(9), 12.17(8) 93.05(15)
V (Å^3)	399(13)	383(9)
Z	2	2
Radiation type	Electron, λ = 0.02510 Å	Electron, λ = 0.02510 Å
Crystal size (μm)	0.5 × 0.3 × ??	0.5 × 0.3 × ??
Data collection		
Diffractometer	XtaLAB Synergy-ED, HyPix-ED, electron source at 200keV	XtaLAB Synergy-ED, HyPix-ED, electron source at 200keV
Scaling	CrysAlis PRO 1.171.43.121a (Rigaku Oxford Diffraction, 2024) Empirical absorption correction using spherical harmonics, implemented in SCALE3 ABSPACK scaling algorithm.	CrysAlis PRO 1.171.43.121a (Rigaku Oxford Diffraction, 2024) Empirical absorption correction using spherical harmonics, implemented in SCALE3 ABSPACK scaling algorithm.
T_{min}, T_{max}	0.644, 1.000	0.875, 1.000
No. of measured, independent and observed [$I \geq 2\mu(I)$] reflections	3886, 1510, 967	1836, 1836, 1479
R_{int}	0.11	0.156
(sin θ_{max}/λ) (Å^{-1})	0.786	0.716
Refinement		
$R[F^2 > 2\sigma(F^2)]$, $wR(F^2)$, S	0.121, 0.283, 1.54	0.162, 0.444, 1.75
No. of reflections	890	1836
No. of parameters	48	61
No. of restraints	66	36
H-atom treatment	H atoms treated by a mixture of independent and constrained refinement	H-atom parameters constrained
$\Delta\rho_{max}$, $\Delta\rho_{min}$ (e Å^{-1})	5.76, –2.14	1.38, –1.27

S3 Magnetic Measurements

Measurements of the magnetic susceptibility were carried out using a Quantum Design Magnetic Property Measurements System XL (MPMS-XL) Superconducting Quantum Interference Device (SQUID) magnetometer. A polycrystalline sample was immobilised in eicosane (masses in Tbl. S7). Magnetic susceptibility measurements were performed under field cooled and zero field cooled conditions in an applied direct current field of 0.01 T over the temperature range $2 - 300$ K. As *M*(H) is linear in this field, the small-field approximation for the susceptibility, $\chi(T) \simeq \frac{M}{H}$, where *M* is the magnetisation and *H* is the magnetic field intensity, was taken to be valid. Data were corrected for diamagnetism of the sample using Pascal's constants.[13] Isothermal magnetisation measurements were carried out at 2 K from -5 to $+5$ T. Summary of fitted parameters in Tbl. S7.

Table S7: Key parameters and measurement details for magnetic measurements

x_{NMR}	Synthesis	mass (mg)	eicosane (mg)	H_{C} (T)	T_{C} (K)	M_r (μ_{B} per Ni)
0.0	solid d_4	22.10	9.22	0.99191(3)	17.5(5)	0.0876(10)
0.0	solid	14.32	14.24	0.8082(2)	17.0(5)	0.0579(10)
0.1071(5)	soln.	17.53	17.77	0.969(3)	15.5(3)	0.0892(10)
0.179(2)	soln.	13.51	13.64	0.6255(18)	15.8(2)	0.0704(10)
0.326(18)	soln.	10.11	10.57	0.373(8)	16.0(5)	0.0485(10)
0.095(6)	solid	16.71	16.84	0.911(18)	17.0(5)	0.0774(10)
0.224(8)	solid	15.75	15.69	0.5306(14)	16.5(2)	0.0686(10)

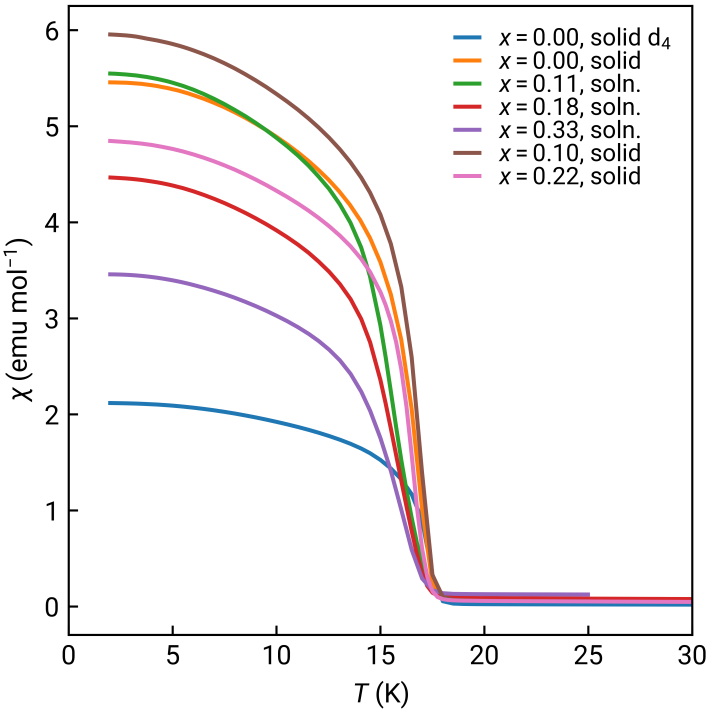

Figure S21: Variation of magnetic susceptibility as a function of temperature $\chi(T)$ M_r for each sample in field cooled conditions.

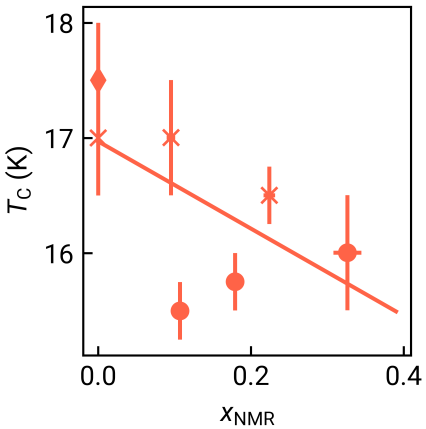

Figure S22: Variation in magnetic ordering temperature T_C with x determined by the maximum in dχ/dT. Circles indicate solution synthesised materials and crosses, solid-state synthesised materials.

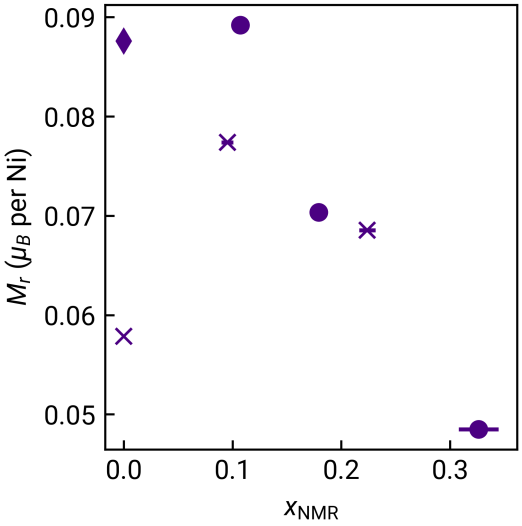

Figure S23: Variation of remnant magnetism M_r with x.

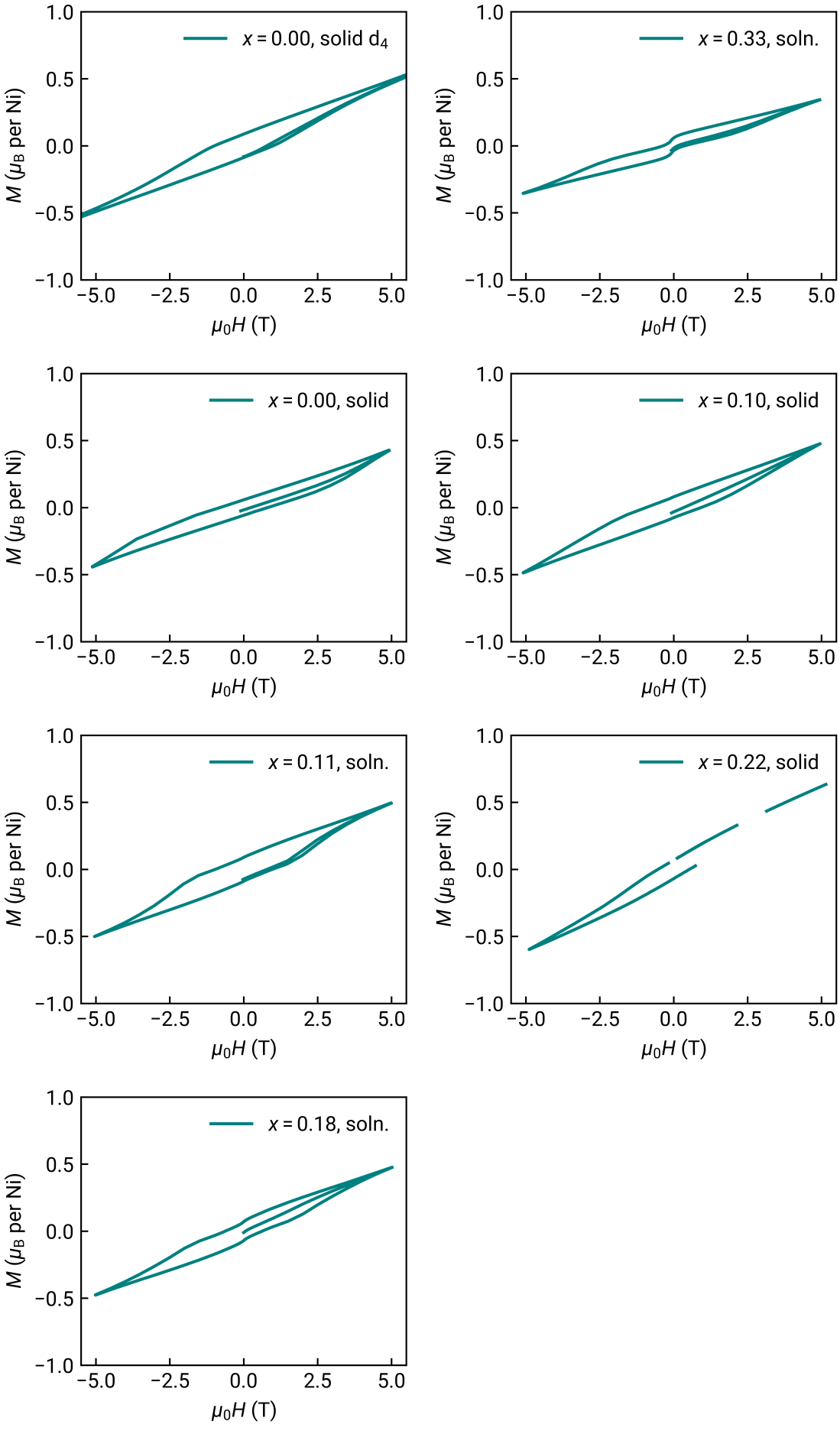

Figure S24: $M(H)$ for each sample.

References

[1] M. L. Evans *et al.*, *J. Open Source Softw.*, 2020, **5**, 2563.
[2] F. Birch, *Phys. Rev.*, 1947, **71**, 809–824.
[3] M. Lertkiattrakul *et al.*, *J. Open Source Softw.*, 2023, **8**, 5556.
[4] A. A. Coelho, *J Appl Cryst*, 2018, **51**, 210–218.
[5] J. Filik *et al.*, *J Appl Cryst*, 2017, **50**, 959–966.
[6] O. V. Dolomanov *et al.*, *J. Appl. Crystallogr.*, 2009, **42**, 339–341.
[7] G. M. Sheldrick, *Acta Crystallogr.*, 2015, **A71**, 3–8.
[8] G. M. Sheldrick, *Acta Crystallogr.*, 2015, **C71**, 3–8.
[9] L. J. Bourhis *et al.*, *Acta Cryst A*, 2015, **71**, 59–75.
[10] A. Saha *et al.*, *Chem. Rev.*, 2022, **122**, 13883–13914.
[11] G. S. Papaefstathiou *et al.*, *J. Solid State Chem.*, 2001, **159**, 371–378.
[12] J. Pitcairn *et al.*, *J. Am. Chem. Soc.*, 2024, **146**, 19146–19159.
[13] G. A. Bain *et al.*, *J. Chem. Educ.*, 2008, **85**, 532.